Towards a Synthetic Tissue Model of the Lower Urinary Tract

Alexander Preis[1] [a], Christina Merkl[1], Paula Miralles[1], Svenja Heer[1], Elisabeth Benke[1] [b],
Sebastian Reitelshöfer[1] [c], Sina Martin[1] [d], Ralf Rieker[2] and Jörg Franke[1] [e]

[1]*Institute for Factory Automation and Production Systems, Friedrich-Alexander-Universität Erlangen-Nürnberg, Germany*
[2]*Institute of Pathology, Universitätsklinikum Erlangen, Friedrich-Alexander-Universität Erlangen-Nürnberg, Germany*

Keywords: Anatomical Model, Urology, Lower Urinary Tract, Urinary Bladder, Urethra, Artificial Urine.

Abstract: The development of medical devices often depends on in vivo studies to validate the proper functioning of the products. These trials provide ethical as well as economic challenges, which can be partially addressed by the usage of realistic synthetic tissue models that replicate human anatomy and the corresponding properties of the biological tissue. In this work, a silicone-based model with a fiber structure and a PVA-based model that exhibits fabrication-induced anisotropy are presented in the special context of the lower urinary tract. The analysis of the materials in the uniaxial tensile test shows the anisotropic and viscoelastic properties of the materials. Furthermore, the anatomical model of the lower urinary tract shows expected deformation in simulation as well as in the real silicone model. Additionally, a suitable artificial urine according to ISO 20696 is shown for use with the model. First experiments to change the pH of the artificial urine are successfully conducted.

1 INTRODUCTION

In the development of medical devices, a large proportion of the costs occur due to elaborate in vivo studies on animals and humans (J. A. DiMasi et al., 2016). As shown in Figure 1, approximately 2.8 million animals were used for research purposes in Germany alone in 2014 (DFG, 2021).

Often previously unknown weaknesses of the tested medical device become apparent in the course of the in vivo test phases, which leads to further iterations, further animal testing and means an economic loss for the companies (I. S. Yoo et al., 2020). In addition, a successful animal test study does not necessarily indicate the suitability of the product for use in humans, as there are sometimes significant differences both anatomically and physiologically (M. Viceconti et al., 2016). To overcome the ethical as well as economic challenges of animal testing, realistic synthetic tissue models that replicate human anatomy and the properties of the biological tissues are an obvious choice.
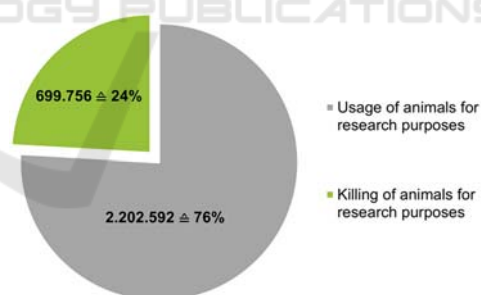

Figure 1: In Germany, approximately 2.8 million animals were used for research purposes in 2014 (DFG, 2021).

In this work, first steps towards a synthetic in-vitro and in-silico tissue model of the lower urinary tract are presented that will be used for the testing of intraurethral artificial urinary spincters like the one presented in (A. Preis et al., 2022).

[a] https://orcid.org/0000-0003-3469-5982
[b] https://orcid.org/0000-0002-6610-4430
[c] https://orcid.org/0000-0002-4472-0208
[d] https://orcid.org/0000-0002-2146-8265
[e] https://orcid.org/0000-0003-0700-2028

1.1 Structure of Biological Tissues

Biological tissues often have unique properties compared to many engineering materials. They are capable of load-dependent adaptation and repair when damaged, which means, that they can adapt to changing mechanical requirements (remodeling). Most biological tissues are complex composite materials with inhomogeneous and anisotropic properties. As a result, the mechanical properties vary from point to point within a tissue and the response to forces acting in different loading directions can be distinct. As an example, the values for the strength and stiffness of bone differ both between various bones and at individual points within the same bone. Furthermore, biological tissues are viscoelastic to a large extent, so the rate of load application and the creep and relaxation processes that occur are also relevant to the analysis of mechanical properties. (Y. C. Fung, 1993)

The mechanical properties of biological tissues, which are mainly composed of cells and an extracellular matrix consisting of fibers and ground substance, are largely determined by the collagen and elastin fiber content. The properties of the tissues are optimized by different compositions and orientations according to the specific application. (Y. C. Fung, 1993)

The primary mechanical function of collagen fibers is to resist axial tension. Because of their large length-to-diameter ratio, they are susceptible to buckling and not suited to withstand compressive loads. When a fiber is pulled, its length increases, as with a mechanical spring, and the energy applied to stretch the fiber is stored. The release of this energy subsequently returns the fiber to its unstretched configuration. The individual fibrils of collagen are surrounded by a gel-like ground substance, which is largely composed of water and contributes to the viscoelastic material behavior with relatively high tensile and low compressive strength of the collagen fibers. Among the non-collagenous tissue components, elastin is another important fibrous protein with material properties comparable to those of rubber. The elastic elastin fibers are highly extensible, and their elongation is reversible even under high stress. They behave elastically with low stiffness up to an elongation of about 200 %, followed by a short range where the stiffness increases sharply until failure. In summary, elastin fibers exhibit elastic material properties with low Young's modulus, while collagen fibers exhibit viscoelastic material behavior with higher Young's modulus. (N. Özkaya et al., 2012)

1.2 Mechanics of Biological Tissues

Viscoelastic materials like biological tissues exhibit both elastic and viscous behavior. In the following, elasticity, viscosity, and viscoelasticity are briefly explained for better understanding.

Elasticity

Elasticity describes the ability of a material or body to reverse a change in shape caused by an external force through its own internal force, which is also referred to as the restoring force. If a specimen with an original length L_0 is loaded longitudinally with a force that deforms the specimen to length L, the strain ε is defined according to (1):

$$\varepsilon = \frac{L - L_0}{L_0} = \frac{\Delta L}{L_0} \tag{1}$$

with:
ε strain
L current length
L_0 initial length
ΔL change in length

Stress σ and strain are related by Hooke's law (2) and are proportional to each other. The proportionality factor is a material constant which is called Young's modulus E.

$$\sigma = E \cdot \varepsilon \tag{2}$$

with:
ε strain
E Young's modulus
σ stress

In models, elastic behavior is usually represented by linear elastic springs. They can deform reversibly when a load is applied and return to their original shape when the load is removed. If a material behaves linearly elastic, the stress is linearly proportional to the strain. In elastic materials, the mechanical properties are independent of time. When externally loaded, they deform instantaneously and return to their original shape almost immediately when unloaded. The fibrous portion of biological tissues can be simplified in such a way. (N. Özkaya et al., 2012)

Viscosity

Viscosity provides information about the flow behavior of a material. The dynamic viscosity η describes the internal friction of fluids and represents the resistance to a forced, irreversible change of location of its volume elements. For a better illustration, one can imagine that the fluid is located

between two plates oriented parallel to each other and adheres to both plates. If the upper plate is moved with a velocity v, the fluid layer in the immediate vicinity also moves with the velocity v due to adhesion. Since the lower plate has not moved, the adjacent fluid layer is at rest. The velocity within the fluid increases from the lower plate at rest to the moving upper plate. In a laminar flow, the velocity gradient dv/dy arises, which is also often abbreviated as $\dot{\gamma}$. For ideal fluids, Newton's law applies to calculate the resulting shear stress τ according to (3):

$$\tau = \eta \, \frac{dv}{dy} = \eta \, \dot{\gamma} \qquad (3)$$

with: τ shear stress
       η dynamic viscosity
       $\dot{\gamma}$ velocity gradient

The dynamic viscosity η acts as a constant of proportionality. Thus, in contrast to elastic solids, the stresses do not depend on the deformation per se, but on the rate of deformation. In models, purely viscous behavior is therefore usually represented by a Newtonian damper. In this model, the resulting stress at a constant viscosity depends only on the deformation rate and the strain rate. The ground substances portion of biological tissues can be simplified as purely viscous. (J. de Vicente, 2012)

Viscoelasticity

Because of their composite structure, biological tissues exhibit both elastic and viscous properties. They therefore exhibit creep and relaxation processes when subjected to loading and unloading. The response of viscoelastic materials depends on the rate at which the load is changed. As a result, the stress-strain diagram of a viscoelastic material also depends on the rate at which the load is applied to the material.

Its behavior can be described by characteristic material functions, which are determined in special experiments, first and foremost the creep and relaxation test. Here, the response of a material to a constant stress applied at time t_0 and removed later at time t_1 is observed. Such a stress immediately causes a strain ε in a linearly elastic material at time t_0. This constant strain remains in the material until time t_1. If the applied stress is removed at time t_1, the linear elastic material immediately and completely recovers from the deformation. To the same constant loading condition, a viscoelastic material responds with strain that gradually increases between times t_0 and t_1. At

time t_1, when the load is removed, a gradual recovery begins.

To represent viscoelastic behavior, models that have springs as well as dampers are used as basic elements. One of the best-known models is the Kelvin-Voigt model, which is based on a parallel connection of the two basic elements. Due to the parallel connection, the strain of the damper equals that of the spring. Using Hooke's law for the elastic spring and Newton's law for the damper, the first order differential equation shown in (4) is obtained (Y. C. Fung, 1993):

$$\sigma = \sigma_H + \sigma_N = E \, \varepsilon + \eta \dot{\varepsilon} \qquad (4)$$

with: σ total stress
       σ_H stress of the spring
       σ_N stress of the damper
       E Young's modulus
       ε strain of the spring
       η dynamic viscosity
       $\dot{\varepsilon}$ deformation rate

The deformation of a damper placed parallel to a spring, as in the Kelvin-Voigt model, is limited by the response of the spring to the applied forces. The damper cannot deform continuously in this arrangement. Therefore, the Kelvin-Voigt model represents a viscoelastic solid behavior. (N. Özkaya et al., 2012)

Another well-known model for simulating viscoelastic behavior is the Maxwell model. Like the Kelvin-Voigt model, it consists of a spring and a damper. However, these are not connected in parallel, but in series. From the arrangement it follows that the total stress of the system must be equal to the stress in the spring and to the stress in the damper. The total strain of the system results from the individual strains of the spring and the damper, as described in (5):

$$\varepsilon = \varepsilon_H + \varepsilon_N = E \, \sigma + \eta \dot{\sigma} = E\eta \dot{\varepsilon} \qquad (5)$$

with: ε total strain
       ε_H strain of the spring
       ε_N strain of the damper
       E Young's modulus
       σ total stress
       η dynamic viscosity
       $\dot{\varepsilon}$ deformation rate

In the case of the Maxwell model, a force application leads to deformation of both the spring and the damper. The deformation of the spring is finite, whereas the damper deforms as long as the force is applied to the system. Therefore, the overall behavior of the Maxwell model resembles a fluid

rather than a solid and is referred to as a viscoelastic fluid model. (N. Özkaya et al., 2012)

However, the Kelvin-Voigt and Maxwell models alone are not capable of representing the real behavior of many viscoelastic materials but can be used to create more complex viscoelasticity models. A well-known one is the Zener model, which is also referred to as the standard linear solid model and can be described by two equivalent representations: the first consists of a series connection of a Kelvin model with a spring, and the second one consists of a parallel connection of a Maxwell model with a spring. It is used to represent the viscoelastic behavior of some biological materials, such as cartilage. Similarly, there is also the three-element fluid model used in the study of blood. In this one, the additional spring is replaced by a damper. Also, other models can be created by combining any number of Maxwell and/or Kelvin-Voigt bodies to represent the behavior of other materials. (N. Özkaya et al., 2012)

2 MATERIALS AND METHODS

In the present work, two possible materials for a synthetic in-vitro tissue model of the lower urinary tract are presented. Additionally, a suited anatomical geometry and a recipe for artificial urine, which can be used to test urinary stone formation, are shown.

2.1 Silicone-Based Model

For the silicone-based model, the RTV-2 silicone "Elastosil P7670 A/B" with a 10 wt% silicone oil (AK 100) content is used (Wacker Chemie AG). To create the anisotropy, additional 'fibers' without silicone oil are embedded in a matrix of silicone according to the previous formula. The silicone is mixed in a vacuum stirrer to avoid air inclusion and subsequently cast into sheets with a thickness of 2 mm and fully cured. The resulting tissue model has a fiber volume content of around 24 %.

2.2 PVA-Based Model

For the PVA-based model, a solution consisting of 10 wt% PVA powder (MW: 133000 g/mol, degree of hydrolysis: 99 %, Polysiences Inc.) in distilled water is prepared. Both components are mixed in a sealed vessel at a constant temperature of 100 °C for a duration of 6 h. The finished, transparent solution is poured into sheets of 2 mm thickness, analogously to the silicone. Any air pockets are removed by vacuum and the plate is cooled to room temperature.

Afterwards it is frozen for at least 16 hours. After the first freezing cycle (consisting of freezing and complete thawing to room temperature), the previously viscous mass has a gelatinous consistency and a whitish color. After two freezing cycles, two opposite ends of the sheet are fixed in a jig, the sheet is stretched by 80 % of its original length and eight more freezing cycles are performed to create the anisotropy. The material is packed airtight to keep the samples from drying out.

2.3 Material Characterization

To determine the mechanical properties of the tissue models, uniaxial tensile tests (Z 2.5/TN1S, ZwickRoell GmbH & Co. KG) are performed with the uniform base materials as well as along and perpendicular to the fiber orientation and strain direction of the anisotropic tissue models. For this purpose, specimen geometry S3A of the DIN 53504 standard is used at strain rates of 200 and 800 mm/min. The significance of the results is then statistically analyzed.

2.4 Lower Urinary Tract

The lower urinary tract consists of the urinary bladder (*vesica urinaria*) and *urethra*. They work together as a functional unit and perform the tasks of storing and emptying urine. In both sexes, the *vesica urinaria* is located in the lesser pelvis just behind the *symphysis*. In women, it lies in front of the *vagina* and in front of and below the *uterus*; in men, it lies in front of the *rectum*. The bladder of an adult has a capacity of about 400 to 500 ml and is emptied to less than 50 ml during micturition. Depending on the state of filling, it is bowl-shaped flattened or spherical. The thickness of the bladder wall varies according to the volume of urine, decreasing accordingly as it expands. The wall thickness ranges from 1 to 5 mm, and can also reach up to 10 mm. The transition from the *vesica urinaria* to the *urethra* is called the bladder neck. The female *urethra* is straight and short, the male *urethra* passes through the *penis* and is longer and has several curves. The female *urethra* considered for this work is about 40 mm long and has a diameter of about 8 mm. (D. Schultz-Lampel et al., 2012; M. Schünke et al., 2022)

The anatomical model of the urinary bladder was created using Autodesk Inventor (Autodesk Inc.). Afterwards the deformation during normal micturition with an abdominal pressure of 20 cmH$_2$O and a detrusor pressure of 30 cmH$_2$O as well as different flow rates with a cumulated intravesical

pressure of 25, 50 and 80 cmH$_2$O were simulated using the multiphysics simulation software Ansys (Ansys Inc.).
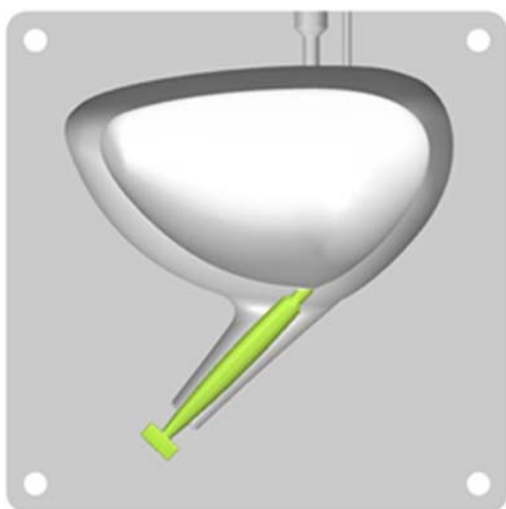

Figure 2: The assembled silicone mold consists of the rigid outer part and inner urethra as well as the inner bladder part made out of wax melting at low temperature.

To manufacture the in-vitro model of the urinary bladder out of silicone, an additive manufactured mold is utilized. While the outer part and the inner urethra are made of rigid material, the inner bladder is made out of wax, which allows the removal by melting after the silicone has been cured. A slice of the assembled mold is shown in Figure 2.

2.5 Artificial Urine

The formation of urinary stones is particularly problematic with foreign bodies inserted in the urinary tract, such as stents, catheters, or the above mentioned intraurethral artificial urinary sphincter. A maximum retention time of two to three months is often recommended for such urinary tract implants. It has been shown that after three or more months, more than 75% of ureteral stents exhibit severe encrustation, making removal of the implant with the standard procedures partially impossible. (T. Kawahara et al., 2012)

As in 'normal' urolithiasis, the formation of the urinary stone here is favored by changes in pH. Classically, infestation also begins by the adsorption of proteins on the implants' surface, which allows subsequent accumulation of bacteria and eventually biofilm formation. This leads to a local change in pH and ultimately to mineral encrustation of the implant. Mainly, the two different mechanisms homogeneous and heterogeneous nucleation can be distinguished.

Homogeneous nucleation results in uric acid and cystin stones caused by an oversaturation of the urine precipitation of the corresponding crystals. On the other hand, heterogeneous nucleation results in calcium and infectious stones caused by detritus or other crystal nuclei, which can be induced by bacterial infection. (R. Hautmann & J. E. Gschwend, 2014)

The formation of the already mentioned three most common main components of urinary stones has different causes:

Oxalate stones are often idiopathic but can also be caused by malnutrition or metabolic defects. Here, both homogeneous and heterogeneous nucleation can be considered.

Uric acid stone formation is increased by more acidic urine since uric acid is poorly soluble in urine with a pH value of less than 6. This can be caused by malnutrition, disease or medication and leads to a homogeneous nucleation.

Phosphate stones are mainly formed in urine with higher pH values above 6.8. The cause of the change in pH is usually an infectious disease of the urinary tract which leads to a local change in pH and therefore a homogeneous nucleation.

It is clearly shown, that changes in pH can have an impact on the formation and type of urine stones. (C. A. Wagner & N. Mohebbi, 2010; H.-U. Schmelz et al., 2014; R. Hautmann & J. E. Gschwend, 2014)

Table 1: Composition of artificial urine (ISO 20696).

CH$_4$N$_2$O	25.0 g
NaCl	9.0 g
Na$_2$HPO$_4$	2.5 g
KH$_2$PO$_4$	2.5 g
NH$_4$Cl	3.0 g
C$_4$H$_7$N$_3$O	2.0 g
Na$_2$SO$_3$ (hydrated)	3.0 g
H$_2$O	1.0 l

Five-fold artificial urine concentrate according to ISO 20696 was acquired from Synthetic Urine e.K. and mixed with distilled water. The composition is detailed in Table 1. Hydrochloric acid (37 %) and sodium hydroxide (20 %) acquired from Algin Chemie e.K. were used to evaluate the titration curve of the artificial urine for future urinary stone formation experiments with changed pH.

3 RESULTS

The results of the uniaxial tension tests of the preliminary tissue models as well as the anatomical

model and the titration curve of the artificial urine are presented in this chapter.

3.1 Properties of the Tissue Models

Figure 3 shows the distribution of elongation at break and tensile strength of the measurements at different test speeds. In case of the silicone-based model, there are 12 valid measurements for the test speed of 200 mm/min and 16 at 800 mm/min. For the PVA-based samples, the number is lower with 8 valid measurements at a test speed of 200 mm/min and 6 at 800 mm/min.
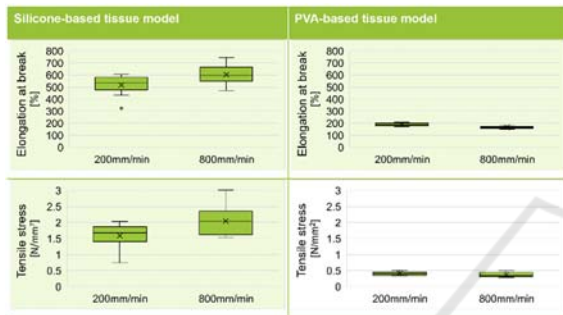

Figure 3: Significant strain rate dependent differences for the materials along fiber direction are highlighted in color.

The statistical analysis of the results shows that for the elongation at break of both models and the tensile strength of the silicone-based tissue model, significant changes in the parameters occur as a function of the test speed. These are highlighted in color in the figure.

Figure 4 shows the distribution of elongation at break and tensile strength of the measurements with loading along and across the preferential direction. The silicone-based model has 16 valid measurements for the test across and 15 along the fiber direction. For the PVA-based specimens, the number is 26 valid measurements across to and 22 along the direction of strain during freezing.
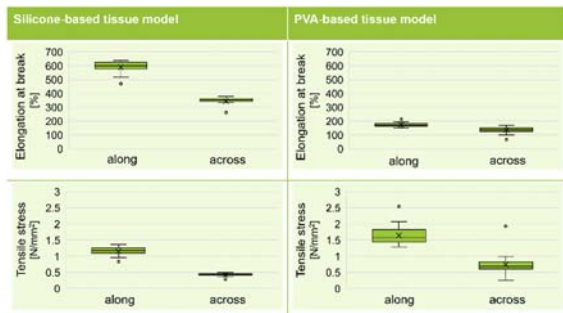

Figure 4: Significant loading direction dependent differences for the materials are highlighted in color.

The statistical analysis of the results shows that for both the elongation at break and the tensile strength of both tissue models significant changes of the parameters occur as a function of the loading direction and thus, as expected, an anisotropy exists. The significant changes are highlighted in color in the figure.

3.2 Discussion of the Tissue Models

The silicone-based tissue model shows a significant increase in values with higher test speed in terms of both elongation at break and tensile strength. Thus, although the stress-strain curve is similar for both strain rates, the tissue model exhibits some viscoelasticity. In addition, significant anisotropy with respect to mechanical properties can also be shown for the model. This is consistent with the theory on fiber composites, according to which the material takes the main load when loaded in fiber direction. (Y. C. Fung, 1993) Due to the high durability of the silicone, the silicone-based tissue model is also well suited for long-term storage and thus is first used for the fabrication of the anatomical lower urinary tract model.

The PVA-based tissue model also shows significant differences in elongation at break depending on the test speed, with the maximum elongation decreasing with increasing loading speed. Although the strength remains the same and shows no significant difference, the decreasing elongation at break still results in a higher slope of the stress-strain curve. The anisotropy test shows significantly higher values for all the material properties investigated for a loading direction corresponding to the loading direction during the freezing and thawing cycles. This is due to the fact that by straining during thermal treatment, the orientation of the PVA-rich phases can be affected (J. L. Holloway et al., 2013). However, the model shows poor long-term stability with changing mechanical properties over time due to the evaporation of water (C. K. McGarry et al., 2020).

3.3 Evaluation of the Anatomical Model

In Figure 5, the simulation of the anatomical model of the lower urinary tract during normal micturition is shown. A consistent abdominal pressure of 20 cmH_2O and an increasing detrusor pressure up to 30 cmH_2O was applied, resulting in a maximum intravesical pressure of 50 cmH_2O. As visible in the figure, the desired bowl shaped deformation is created.
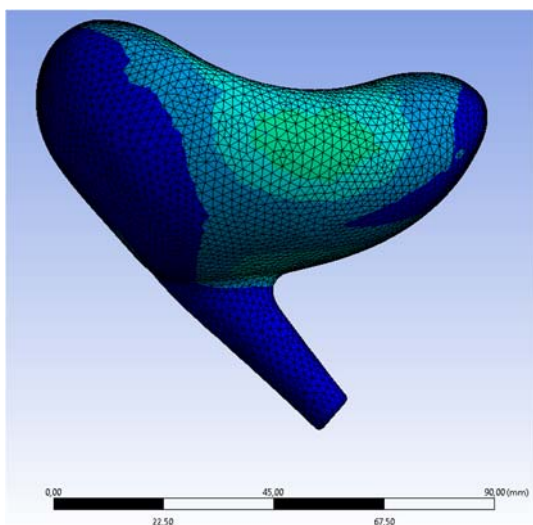
Figure 5: Deformation of the bladder after normal micturition with a detrusor pressure of 30 cmH$_2$O.

The flow rate was simulated utilizing different intravesical pressures between 25 and 80 cmH$_2$O. As shown in Table 2, the resulting flow rates of 22.81, 28.87 and 34.97 ml/s are within the physiological values of 20 to 35 ml/s (D. Schultz-Lampel et al., 2012).

Table 2: The simulated flow rates caused by different intravesical pressures are within the physiological range of 20 to 35 ml/s (D. Schultz-Lampel et al., 2012).

Intravesical pressure in cmH$_2$O	Flow rate in ml/s
25	22.81
50	28.87
80	34.97

The bladder model manufactured out of silicone is shown in Figure 6. Here, different fill volumes of 50, 100, and 500 ml are shown. The resulting deformations reflect the results of the simulation as well as the one of the real urinary bladder.
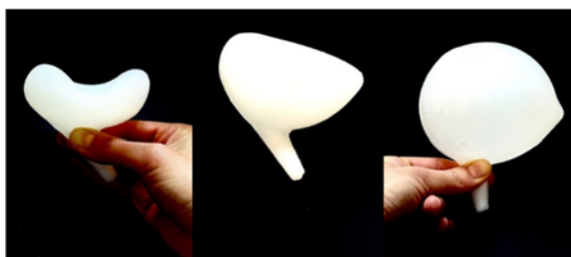

Figure 6: The silicone bladder model filled with 50, 100, and 500 ml (left to right) shows realistic deformation.

3.4 pH Change of the Artificial Urine

Figure 7 shows the titration curve of the artificial urine with its pH decreased by adding 37 % HCl and increased by addition of 20 % NaOH. When comparing the pH decrease with the pH increase by a pH difference of 5, it is noticeable that the amount of HCl used is 0.39% higher by volume than for NaOH.
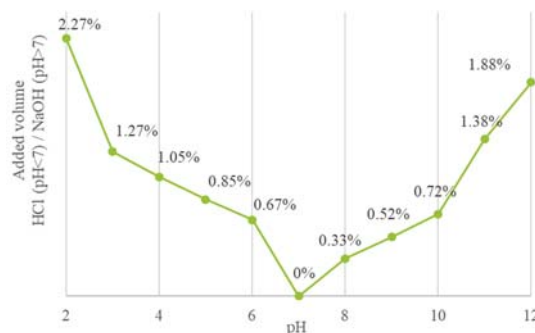

Figure 7: Comparison of titration curves for the addition of 37 % HCl (pH < 7) and 20 % NaOH (pH > 7) in volume percent.

4 SUMMARY AND OUTLOOK

To avoid relying on samples of human or animal origin, it is desirable to have a synthetic tissue model that exhibits proper material behavior and is a sufficient representation of the real human anatomy. Silicone-based models with a fiber structure and PVA-based models that exhibit fabrication-induced anisotropy are both suitable for this purpose. The analysis of the materials in the uniaxial tensile test at 200 mm/min and 800 mm/min strain rate shows the viscoelasticity of the base materials of the models.

Due to the room temperature vulcanization, the silicone can be easily mixed and poured into any mold. Furthermore, by adjusting the base silicone as well as silicone oil and fiber content in the model, the mechanical properties of the material can be adjusted in future work, allowing the targeted replication of specific tissue types. The fiber orientation makes the anisotropy of the model readily adjustable. It thus offers the possibility of replicating tissue structures that exhibit strong fiber orientation, such as skeletal muscle. Because of this, the material was chosen to create the in-vitro model of the lower urinary tract.

The manufacturing process of the PVA-based model is simple and the mechanical properties can be adjusted in many ways. This enables the modeling of a wide range of biological tissues. In addition, anisotropic properties could be generated even for

more complex geometries, as this is dependent on the load during the freezing cycles. In the case of the human urinary bladder, the load could be applied by inflation. However, since the mechanical properties of the PVA-based model change over time due to the evaporation of water, it is not suitable for long-term storage.

Additionally, an anatomical model of the female human lower urinary tract is presented. The model is created with ease of manufacturing in mind. Openings for *ureters* can be added after casting. Simulation utilizing Ansys shows, that the deformation of the created in-silico model during micturition represents the normal bowl shaped deformation of the real counterpart. The manufactured in-vitro silicone model also shows the fitting deformation during filling and micturition.

After implantation of an intraurethral artificial urinary sphincter like the one presented by (A. Preis et al., 2022) into the lower urinary tract model, artificial urine using the recipe of ISO 20696 can be used to test for possible urinary stone formation caused by the implant. The titration curve of the urine using hydrochloric acid and sodium hydroxide is shown and will be used to modify the pH and thus check for different urinary stone formation situations.

In future work, the results will be used as a starting point to create a realistic mechatronic urodynamic test bench, which can be used to test the already presented purely mechanical intraurethral artificial urinary sphincter. The main components that need to be addressed are the material properties of the bladder, the urethra and the method of mechatronisation of the test bench to create the wanted urodynamic conditions.

REFERENCES

C. A. Wagner, & N. Mohebbi (2010). Urinary pH and stone formation. *Journal of Nephrology*. https://doi.org/10.5167/uzh-45805

C. K. McGarry, L. J. Grattan, A. M. Ivory, F. Leek, G. P. Liney, Y. Liu, P. M., R. Rai, A. P. Robinson, A. J. Shih, B. Zeqiri, & C. H. Clark (2020). Tissue mimicking materials for imaging and therapy phantoms: a review. *Physics in Medicine and Biology*. https://doi.org/10.1088/1361-6560/abbd17

D. Schultz-Lampel, M. Goepel, & A. Haferkamp. (2012). *Urodynamik* (3., vollst. bearb. Aufl.). Springer Medizin.

DFG. (2021). *Tierversuche in der Forschung*. https://www.dfg.de/download/pdf/dfg_im_profil/gesch aeftsstelle/publikationen/tierversuche_forschung.pdf

H.-U. Schmelz, C. Sparwasser, & W. Weidner. (2014). *Facharztwissen Urologie*. Springer.

I. S. Yoo, A. Preis, & J. Franke (2020). Development of a test bench for the urodynamic simulation of the lower urinary tract. https://doi.org/10.1109/EMBC44109.2020.9176198

J. A. DiMasi, H. G. Grabowski, & R. W. Hansen (2016). Innovation in the pharmaceutical industry: New estimates of R&D costs. *Journal of Health Economics*. https://doi.org/10.1016/j.jhealeco.2016.01.012

J. de Vicente (Ed.). (2012). *Viscoelasticity - From Theory to Biological Applications*. IntechOpen Limited. https://doi.org/10.5772/3188

J. L. Holloway, A. M. Lowman, & G. R. Palmese (2013). The role of crystallization and phase separation in the formation of physically cross-linked PVA hydrogels. *Soft Matter*. Advance online publication. https://doi.org/10.1039/C2SM26763B

M. Schünke, E. Schulte, & U. Schumacher. (2022). *PROMETHEUS: LernAtlas Anatomie*. Thieme.

M. Viceconti, A. Henney, & E. Morley-Fletcher (2016). In silico clinical trials: how computer simulation will transform the biomedical industry. https://doi.org/10.13140/RG.2.1.2756.6164

N. Özkaya, M. Nordin, D. Goldsheyder, & D. Leger. (2012). *Fundamentals of Biomechanics*. Springer.

A. Preis, J. Treviranus, E. Benke, S. Reitelshöfer, & J. Franke (2022). Novel Concept for a Mechanical Intraurethral Artificial Urinary Sphincter. *Proceedings of the 15th International Joint Conference on Biomedical Engineering Systems and Technologies - BIODEVICES*. https://doi.org/10.5220/0010885700003123

R. Hautmann, & J. E. Gschwend. (2014). *Urologie*. Springer.

T. Kawahara, H. Ito, H. Terao, M. Yoshida, & J. Matsuzaki (2012). Ureteral stent encrustation, incrustation, and coloring: morbidity related to indwelling times. *Journal of Endourology*. https://doi.org/10.1089/end.2011.0385

Y. C. Fung. (1993). *Biomechanics: Mechanical Properties of Living Tissues* (2nd ed.). Springer.